ACS APPLIED MATERIALS & INTERFACES
Research Article
www.acsami.org

The Role of Cesium Cation in Controlling Interphasial Chemistry on Graphite Anode in Propylene Carbonate-Rich Electrolytes

Hongfa Xiang,[†,∥] Donghai Mei,[‡] Pengfei Yan,[§] Priyanka Bhattacharya,[†] Sarah D. Burton,[§] Arthur von Wald Cresce,[⊥] Ruiguo Cao,[†] Mark H. Engelhard,[§] Mark E. Bowden,[§] Zihua Zhu,[§] Bryant J. Polzin,[#] Chong-Min Wang,[§] Kang Xu,[⊥] Ji-Guang Zhang,[†] and Wu Xu*[,†]

[†]Energy and Environment Directorate, [‡]Fundamental and Computational Sciences Directorate, and [§]Environmental and Molecular Sciences Laboratory, Pacific Northwest National Laboratory, Richland, Washington 99354, United States

[∥]School of Materials Science and Engineering, Hefei University of Technology, Hefei, Anhui 230009, People's Republic of China

[⊥]Sensor and Electron Devices Directorate, U.S. Army Research Laboratory, Adelphi, Maryland 20783, United States

[#]Chemical Sciences and Engineering Division, Argonne National Laboratory, Argonne, Illinois 60439, United States

Supporting Information

ABSTRACT: Despite the potential advantages it brings, such as wider liquid range and lower cost, propylene carbonate (PC) is seldom used in lithium-ion batteries because of its sustained cointercalation into the graphene structure and the eventual graphite exfoliation. Here, we report that cesium cation (Cs^+) directs the formation of solid electrolyte interphase on graphite anode in PC-rich electrolytes through its preferential solvation by ethylene carbonate (EC) and the subsequent higher reduction potential of the complex cation. Effective suppression of PC-decomposition and graphite-exfoliation is achieved by adjusting the EC/PC ratio in electrolytes to allow a reductive decomposition of Cs^+-$(EC)_m$ ($1 \leq m \leq 2$) complex preceding that of Li^+-$(PC)_n$ ($3 \leq n \leq 5$). Such Cs^+-directed interphase is stable, ultrathin, and compact, leading to significant improvement in battery performances. In a broader context, the accurate tailoring of interphasial chemistry by introducing a new solvation center represents a fundamental breakthrough in manipulating interfacial reactions that once were elusive to control.

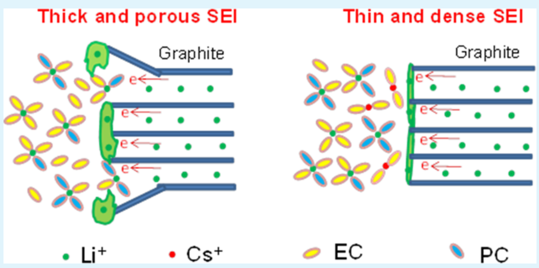

KEYWORDS: *graphite exfoliation, propylene carbonate, solid electrolyte interphase, cesium cation, electrolyte*

1. INTRODUCTION

Lithium-ion batteries (LIBs) have achieved significant success in consumer electronic devices since 1991 and, in recent years, have begun to penetrate applications in hybrid or pure electric vehicles. An overwhelming majority of state-of-the-art LIBs still use graphite as the anode material, with diversified cathode chemistries based on lithium transition metal oxides or phosphates, and electrolytes based on carbonate solutions of lithium hexafluorophosphate ($LiPF_6$). Given the negative potential of the graphite anode (~0.2 V vs Li), the ad hoc solid electrolyte interphase (SEI) formed on the graphite anode surface is the critical component that supports the reversible Li^+-intercalation/deintercalation chemistry involved. Ethylene carbonate (EC) has been identified as the indispensable ingredient responsible for providing such a protective interphase.[1] However, the high melting point of EC (36.4 °C) imposes a narrow service temperature range on most LIBs. The replacement of EC with propylene carbonate (PC) could lead to a great performance improvement in service temperature range because of the low melting point of PC (−48.8 °C). However, the inability of PC to form a protective SEI has significantly restricted its use in electrolytes (<10%). More often than not, additives that assist in forming an SEI have to be used in addition to PC. This approach leads to thicker SEI layers that negatively compromise important characteristics such as rate capability, low-temperature performance, and cycling stability at elevated temperatures.

A key factor that dictates the SEI chemical composition has been identified as the Li^+-solvation structure (i.e., Li^+-$(sol)_n$ solvate) in which the solvent molecules act as the primary SEI building blocks.[2−5] Using high Li^+ concentrations[6−8] or adding calcium cation (Ca^{2+})[9,10] in electrolytes has been reported to alter Li^+-solvation sheath structure and suppress graphite exfoliation caused by PC- or dimethyl sulfoxide-based electrolytes. However, high viscosity and low ionic conductivity inevitably brought by the high salt concentration (>2 mol kg^{-1}) rendered them impractical for low-temperature applications.

Here, we demonstrate that it is possible to direct the formation chemistry of SEI by using cesium cation (Cs^+) at additive concentrations, whose preferential coordination with EC, along with the higher reduction potential of the resultant complex cation, leads to an EC-originated SEI on the graphite

Received: June 22, 2015
Accepted: September 1, 2015
Published: September 10, 2015

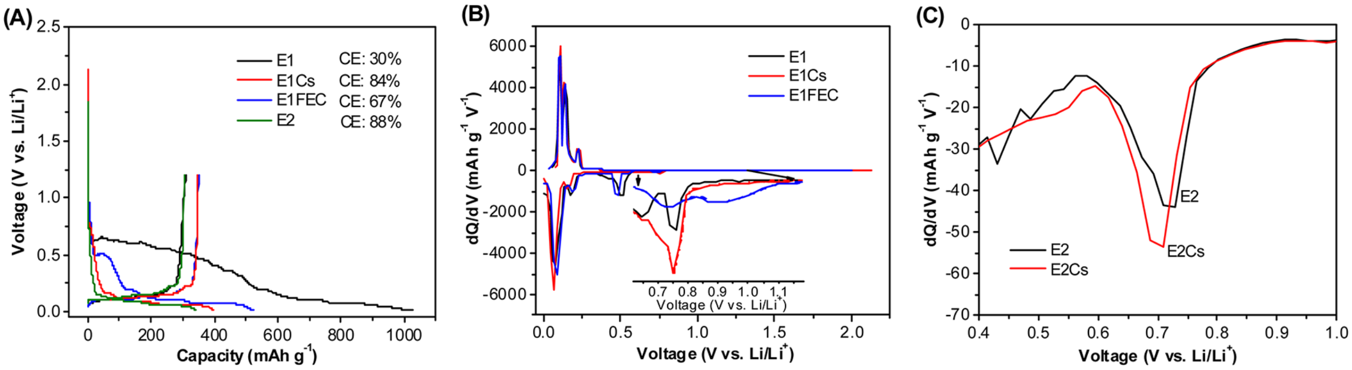

Figure 1. Electrochemical behavior of various $LiPF_6$−$CsPF_6$ electrolytes on graphite surfaces. (A) Lithiation/delithiation profiles of Li|graphite half cells using electrolytes of E1, E1Cs, E1FEC, and conventional E2. (B and C) Comparison of differential capacity (dQ/dV) plots of Li|graphite cells using electrolytes of E1, E1Cs, and E1FEC (B), and E2 and E2Cs for the 0.75 V peak (C).

surface despite the dominant PC population in the electrolyte bulk. This approach of exercising precise control over the SEI formation chemistry assisted by an added foreign cation resolves the incompatibility between the graphite anode and the PC-rich electrolyte while avoiding undesired impact on electrolyte bulk properties. It opens an entirely new avenue for enabling improved LIB performance that is otherwise impossible when using conventional electrolytes.

2. EXPERIMENTAL SECTION

Materials. $LiPF_6$, lithium bis(trifluoromethanesulfonyl)imide (LiTFSI), EC, PC, ethyl methyl carbonate (EMC), and vinylene carbonate (VC) of battery grade were ordered from BASF Battery Materials and were used as received. Fluoroethylene carbonate (FEC) was purchased from Solvay Chemicals. Cesium hexafluorophosphate ($CsPF_6$, ≥99.0%) and cesium bis(trifluoromethanesulfonyl)imide (CsTFSI, ≥99.5%) were purchased from SynQuest Laboratories (Alachua, FL) and Solvionic (France), respectively. Both salts were dried at 65 °C for 4 days under vacuum inside the antechamber of an argon-filled glovebox (MBraun). Coated graphite (MAG-10, 1.53 mAh cm^{-2}) and $LiNi_{0.80}Co_{0.15}Al_{0.05}O_2$ (NCA, 1.50 mAh cm^{-2}) electrodes were provided by the CAMP Facility at Argonne National Laboratory. The compositions of the electrodes are summarized in Table S1. High-purity Li chips with dimensions of 15.6 mm in diameter and 0.45 mm in thickness were purchased from MTI Corp. Various electrolyte solutions were prepared in the glovebox, and the electrolyte formulations are listed in Table S2. All ratios or percentages indicated in this Article are based on weight except otherwise specified.

Electrochemical Measurements. The electrochemical properties of various electrolytes were evaluated in 2325-type coin cells (National Research Council Canada), including Li|graphite half cells and graphite|$LiNi_{0.80}Co_{0.15}Al_{0.05}O_2$ (i.e., graphite|NCA) full cells. Both graphite and NCA electrode laminates were punched into discs (Φ14 mm) for assembling the cells. The mass loadings in each graphite and NCA electrodes were 16.0 and 7.8 mg, respectively. Polyethylene microporous membrane from Celgard was used as the separator. The amounts of electrolytes in the Li|graphite half cells and the graphite|NCA full cells were 80 and 100 μL, respectively. The electrochemical properties of the cells were evaluated on an Arbin BT2000 battery testing station. Galvanostatic charge−discharge tests were performed under different current rates, in which 1C corresponds to a current density of 1.5 mA cm^{-2}. For the half cells and the full cells, the cutoff voltages were set at 0.005 to 1.2 V and 4.3 to 2.5 V, respectively. The cycling stability at elevated temperature (60 °C) and low-temperature discharge performance of graphite|NCA full cells were tested in a Tenney JR environmental chamber. For all of the full cells, two formation cycles were initially conducted at a 0.05C rate for both charge and discharge processes at room temperature, and, subsequently, the cycling performance, discharge performance, or rate capability was evaluated at various temperatures and current densities. The electrochemical impedance spectrum of the coin cells was measured on a Solartron 1255B frequency response analyzer controlled by Zplot software with a 10-mV perturbation in the frequency range from 10^6 to 10^{-1} Hz.

Characterization. Graphite electrodes were removed from the Li|graphite half cells charged (i.e., Li insertion) to 0.3 V and the graphite|NCA full cells after 100 cycles at 60 °C in the argon-filled glovebox. Subsequently, these graphite electrodes were rinsed five times with EMC to remove the residual electrolytes and dried in the vacuum chamber of the glovebox. ^{17}O nuclear magnetic resonance (NMR) was recorded on a 500 MHz Varian Inova console using a 5 mm DB Nalorac probe tuned to 67.8 MHz. A single pulse experiment without H decoupling was used. The spectral width was 100 kHz, the pulse width 90 was 15 μs, the recycle delay was 0.2 s, and 5000 or 10000 scans were collected for each spectrum. The temperature was 50 °C for all samples except D_2O. D_2O was used to determine the ^{17}O rf pulse width and set the chemical shift reference to zero when at 25 °C. The electrospray ionization mass spectrometry (ESI−MS) was conducted on a JEOL AccuTOF. Electrolyte samples were put into the injection system neat, meaning that no acetonitrile or methanol was used as a cosolvent. The injector was a needle with an inner diameter of ∼250 um and an outer diameter of 1.5 mm, and was used to inject the electrolyte into the ionization chamber with a flow rate of 500 uL/min at ambient pressure. The needle was biased to 3100 V, while the mass spectrometer orifice was biased to 20 V. The mass spectrometer orifice was located 3 cm from the injector needle. The data from the entire available mass range, from m/z = 20 to 1000, were collected.

For scanning electron microscopy (SEM), X-ray photoemission spectra (XPS), and time-of-flight secondary ion mass spectrometry (ToF-SIMS) characterizations, the electrodes were used directly. For micro-X-ray diffractometer (micro-XRD) and transmission electron microscopy (TEM) analyses, the graphite composite powders along with the binder were scraped from the copper current collector. SEM images were collected in an FEI Quanta FESEM at an accelerating voltage of 5 kV. XPS measurements were performed on a Physical Electronics Quantera scanning X-ray microprobe using a focused monochromatic Al Kα X-ray (1486.7 eV) source for excitation and a spherical section analyzer. Microbeam micro-XRD was characterized on a Rigaku D/MAX-2000 using Cr Kα radiation with an operating voltage and current of 40 kV and 30 mA, respectively. For micro-XRD measurements, all of the samples were sealed in the capillaries in the glovebox. SEM images and the corresponding energy dispersive X-ray spectroscopy (EDS) analysis of the Li electrodes for both the surface and the cross section were obtained with a JEOL 5800 microscope with Oxford EDS/EDAX. To avoid electrode contamination or side reactions with atmospheric moisture and oxygen, the samples were transferred from the glovebox to the SEM and XPS in sealed vessels that were filled with argon gas.

Computational Calculations. Density functional theory calculations were performed using the generalized gradient approximation

DOI: 10.1021/acsami.5b05552
ACS Appl. Mater. Interfaces 2015, 7, 20687−20695

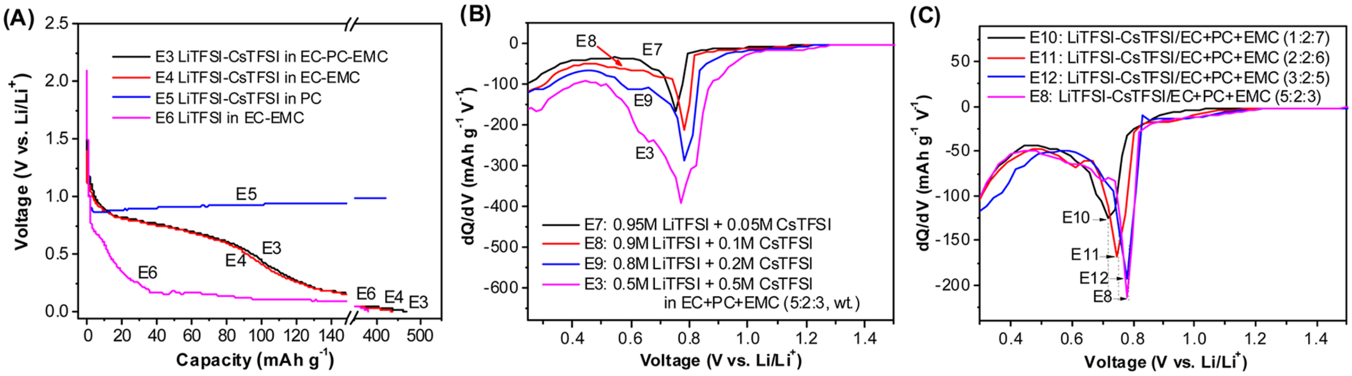

Figure 2. Electrochemical behavior of various LiTFSI−CsTFSI electrolytes on graphite surfaces. (A) Initial lithiation profiles of graphite in different carbonate electrolytes. (B and C) Comparison of the 0.75 V reduction peaks via dQ/dV plots for EC−PC−EMC (5:2:3 by wt) electrolytes at different Cs^+ concentrations (B) and various electrolytes containing 0.9 M LiTFSI and 0.1 M CsTFSI in different EC−PC−EMC mixtures (C). The current density for both lithiation and delithiation was 0.075 mA cm^{-2} (C/20 rate).

as implemented in the Gaussian 09 suite of programs.[11] The B3LYP functional combined with the 6-311++G(d,p) basis set was used in geometry optimization calculations.[12,13] Vibrational frequencies were computed for yielding zero-point energy and thermal corrections. Gibbs free energies were calculated at 298.15 K. The solvent effect was addressed by optimizing the molecular geometries at the same level of theory using the PCM model with EC bulk solvent (dielectric constant = 89.78). The coordination number of Li^+ or Cs^+ was determined by the Gibbs reaction energy.

$$\Delta G = G[M^+(\text{solvent})_n] - G[M^+(\text{solvent})_{n-1}] - G[\text{solvent}]$$

where M is Li or Cs; solvent is EC or PC.

3. RESULTS AND DISCUSSION

Electrochemical Behavior of Cs^+ in the Li|Graphite Half Cells. The electrode compositions and the electrolyte formulations used in this work are summarized in Tables S1 and S2. To evaluate how Cs^+ affects the interphasial chemistry at the graphite surface in PC-rich electrolytes, we studied 1.0 M $LiPF_6$ electrolytes in EC−PC−EMC (5:2:3 by wt) both with and without 0.05 M $CsPF_6$ (denoted as E1Cs and E1, respectively) in Li|graphite half cells. As a comparison, FEC, commonly used as a fluorine source for effective SEI formation also was added at 2 wt % (or 0.25 M) into E1 (E1FEC). As shown in Figure 1A, E1 exhibits a long plateau above 0.5 V indicating extensive PC reduction and subsequent graphite exfoliation. This plateau is apparently suppressed in the presence of FEC, but it does not disappear completely; in contrast, 0.05 M $CsPF_6$ completely inhibits this parasitic process. The Cs^+-effect is more obvious quantitatively in the first cycle irreversible capacities (16% for E1Cs, 33% for E1FEC, and 60% for E1), which is comparable to the 10−12% for the state-of-the-art electrolyte in the absence of PC (1.0 M $LiPF_6$ in EC−EMC 3:7 by vol., E2). In other words, 0.05 M $CsPF_6$ functions much more effectively in suppressing PC interfacial reactions than 2% FEC. Differential capacity plots in Figure 1B provide a more visual comparison, in which the observed conspicuous cathodic peaks at ∼0.5 V in E1 or E1FEC, attributed to the PC-reduction process at the graphite, would disappear when Cs^+ is present. Closer examination of the cathodic curves between 1.1 and 0.7 V reveals a small reductive peak at 0.75 V for all three electrolytes. We speculate that this peak corresponds to the electrochemical reduction of EC molecules in the Li^+-$(EC)_n$ solvates, which should be destined to be part of the SEI formed. For E1FEC, a third cathodic peak at a higher potential (∼0.95 V) is attributed to the reduction of FEC, which should be responsible for forming an F-containing interphase. With the SEI film formed by FEC, the reductive decomposition of EC at 0.75 V is significantly suppressed; however, the peak area or the irreversible capacity corresponding to the peak at 0.75 V for E1Cs is slightly higher than others, indicating that Cs^+ in E1Cs somehow directs a bit more EC into the reduction process. The same phenomenon also is observed in E2Cs, although at a much smaller magnitude, probably because of the absence of PC (Figure 1C).

To reveal the correlation between EC reduction and Cs^+ content, we replaced $CsPF_6$ with its more soluble derivative CsTFSI in LiTFSI-carbonate electrolytes, so that the limited solubility (∼0.06 M) of $CsPF_6$ in carbonate solvents could be circumvented.[14] Thus, in formulations containing various ratios of EC and PC, electrolytes with high concentrations of CsTFSI (E3−E6) can be easily prepared. Figure 2A shows the effects of bulk solvent composition on the lithiation behavior of graphite during the first cycle. It is apparent that the PC-rich E3 exhibits the same electrochemical characteristics with PC-free E4. When comparing EC-free E5 and Cs^+-free E6 with E3 and E4, it becomes apparent that the plateau averaged at about 0.75 V in E3 and E4 should relate mainly to Cs^+ and EC. The quantitative correlation between Cs^+ concentration and electrochemistry is shown in Figure 2B. The same cathodic peak at 0.75 V observed for E1Cs is also seen in E7 at 0.05 M CsTFSI. When the CsTFSI concentration is increased to 0.1 M (E8) and above such as 0.2 M (E9) and 0.5 M (E3), this peak gradually shifts to 0.8 V, with an accompanying intensity increase. The shift probably results from the change of SEI source. In E7 and E1Cs, which have a low Cs^+ content (0.05 M), the SEI-precursors are mainly Li^+-$(sol)_n$ and partly Cs^+-$(sol)_m$ complex cations ($1 \leq n, m \leq 5$). In the electrolytes with higher Cs^+ concentrations, however, Cs^+-$(sol)_m$ solvates become the main source for the interphasial reactions because of the sheer population and the possible higher reduction potential of Cs^+-$(sol)_m$ than Li^+-$(sol)_n$ (see the discussions about the molecular energies of the solvates in the next section). On the other hand, if the EC content is higher, the process occurred at 0.75 V shifts to higher potentials with the intensity increasing in the order of E8 > E12 > E11 > E10 (Figure 2C), demonstrating that the electrochemical reduction of EC in solvation sheaths of both Li^+ and Cs^+ should be responsible for the process. Normally the peak intensity or peak area is an indication of the reaction amount of the corresponding compounds. It is therefore indicated that with

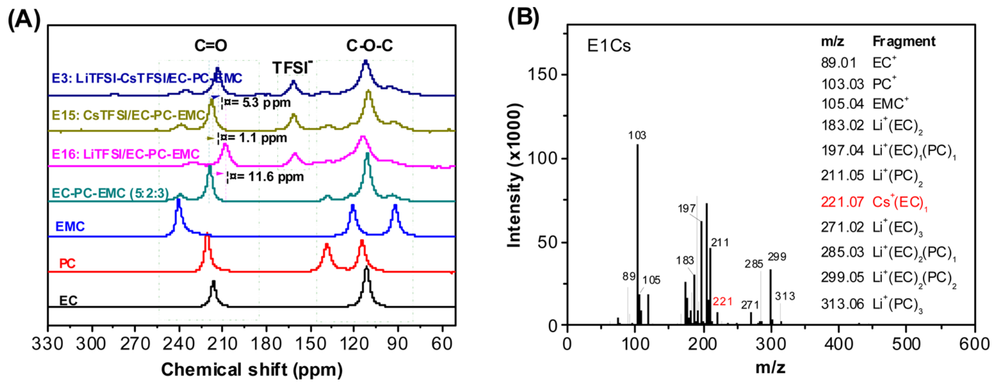

Figure 3. (A) ^{17}O NMR spectra of various solvents and electrolytes. (B) ESI−MS results of electrolyte E1Cs.

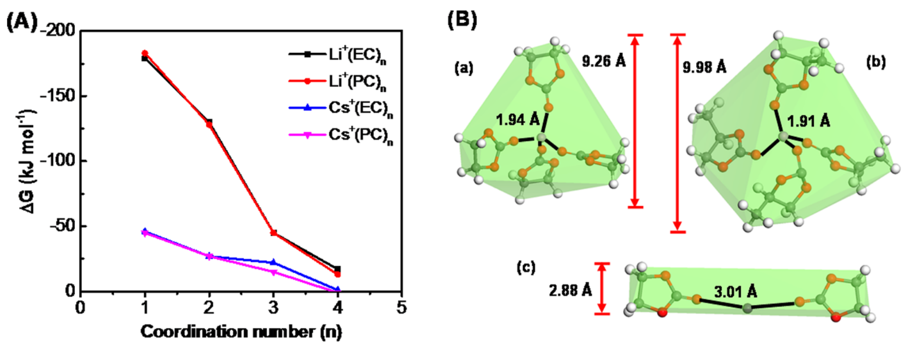

Figure 4. Computational calculations for several cation-solvent solvates in the liquid phase at the level of B3LYP/6-311++G(d,p). (A) Variation of solvation energy with coordination number for Li^+-$(sol)_{n=1-4}$ and Cs^+-$(sol)_{n=1-4}$ (where sol = EC, PC). (B) Comparison of optimal structures of selected solvates: (a) Li^+-EC_4, (b) Li^+-PC_4, and (c) Cs^+-EC_2.

the increase of Cs^+ or EC amount in the electrolyte, more of the solvates Cs^+-$(EC)_m$ will be irreversibly reduced at about 0.75−0.8 V to form SEI layer on graphite during the first charge process.

Protective Mechanism of Cs^+ on Graphite in the PC-Containing Electrolytes. With ESI−MS and ^{17}O NMR, Xu and co-workers have established that cyclic carbonate solvents (EC and PC) with high dielectric constants are preferred by Li^+ over acyclic carbonates (EMC in this work) when forming a solvation sheath.[4,5,15−17] Hence, the resultant SEI would most likely bear chemical signatures of cyclic rather than acyclic carbonate molecules. Furthermore, between the two cyclic solvents PC and EC, Li^+ prefers PC.[17] In this work, we measured Li^+-solvation sheath structures in E1Cs and other reference electrolytes with both ^{17}O NMR and ESI−MS, and the results are shown in Figure 3 and Figure S1.

The ^{17}O NMR results (Figure 3A) reveal that Cs^+ causes much less displacement in the C═O chemical shift ($\Delta\delta$ = 1.1 ppm) than does Li^+ ($\Delta\delta$ = 11.6 ppm). This indicates that Cs^+ acts as a much weaker Lewis acid, and its solvation number with cyclic carbonate solvents should be lower than that of Li^+, which is consistent with literature reports that the coordination number for Li^+ in nonaqueous solvents is normally ∼4[1,18−23] and for Cs^+ is <2.[2] One would infer that, in competition with Li^+ for cyclic carbonate molecules, Cs^+ would most likely lose.

Results from ESI−MS analysis of E1Cs (Figure 3B) shows a strong peak at m/z of 221, demonstrating the dominant existence of Cs^+-$(EC)_1$; however, no Cs^+-$(PC)_1$ (m/z 235) is detected, although both this solvate and Cs^+-$(PC)_2$ (m/z 337) have been detected in E13 when there is no EC in the solution (Figure S1A). To clarify whether Cs^+ prefers EC over PC, E14 was formulated to be Li^+-free with sufficient populations of both PC and EC available. The conclusion is unambiguous: Cs^+ prefers PC over EC (Figure S1B) just like Li^+ reported by Xu and co-workers.[17] Thus, the absence of Cs^+-$(PC)_n$ in E1Cs, in which the molar ratio of Li^+:Cs^+:EC:PC:EMC is 1:0.05:6.49:2.24:3.30 and the PC population is barely sufficient to solvate Li^+, is clearly the result of Li^+-competition. In other words, in such PC-rich electrolytes, Li^+ acts like a PC-scavenger, while Cs^+, losing the competition for PC molecules, would be primarily solvated by EC molecules. As indicated by Xu and co-workers,[17,24] the solvation numbers and compositions for the solvation sheath structure revealed by ESI−MS technique are normally smaller than those from time-averaged spectroscopic techniques such as Fourier transform infrared, Raman, and NMR spectroscopy; however, the solvation sheath structures as revealed by ESI−MS are closer to those of the primary sheath, where the solvents are most tightly bound to Li^+.

Theoretical calculations were conducted on binding energies of Li^+-$(sol)_n$ and Cs^+-$(sol)_m$ solvates (where $1 \le m, n \le 4$) using density functional theory. The results of these calculations are shown in Figure 4A and Figure S2. Cs^+-$(sol)_m$ solvates demonstrate lower binding energies than Li^+-$(sol)_n$ under the same coordination number. On the basis of the ESI−MS results described above and the literature, we chose the coordination numbers 3 and 4 for Li^+-$(sol)_n$ solvates and 1 and 2 for Cs^+-$(sol)_m$ solvates. The optimized structures are shown in Figure 4B and Figures S3−S6. As shown in Table 1, energies of the lowest unoccupied molecular orbitals (LUMO) for both Cs^+-$(EC)_1$ and Cs^+-$(EC)_2$ are much lower than those of Li^+-$(EC)_a(PC)_b$, where $0 \le a, b \le 4$, and $a + b$ = 3 or 4. The

DOI: 10.1021/acsami.5b05552
ACS Appl. Mater. Interfaces 2015, 7, 20687−20695

Table 1. LUMO Energies of Selected Solvates

no.	name	E_{LUMO} (eV)	no.	name	E_{LUMO} (eV)
1	$Li^+(EC)_1$	−5.12	15	$Cs^+(EC)_1$	−4.30
2	$Li^+(EC)_2$	−3.45	16	$Cs^+(EC)_2$	−3.51
3	$Li^+(EC)_3$	−2.77	17	$Cs^+(EC)_3$	−2.81
4	$Li^+(EC)_4$	−2.11	18	$Cs^+(EC)_4$	−2.20
5	$Li^+(PC)_1$	−5.06	19	$Cs^+(PC)_1$	−4.27
6	$Li^+(PC)_2$	−3.23	20	$Cs^+(PC)_2$	−3.44
7	$Li^+(PC)_3$	−2.50	21	$Cs^+(PC)_3$	−2.72
8	$Li^+(PC)_4$	−1.95	22	$Cs^+(PC)_4$	−2.08
9	$Li^+(EC)_1(PC)_1$	−3.34	23	$Cs^+(EC)_1(PC)_1$	−3.48
10	$Li^+(EC)_1(PC)_2$	−2.54	24	$Cs^+(EC)_1(PC)_2$	−2.75
11	$Li^+(EC)_1(PC)_3$	−1.98	25	$Cs^+(EC)_1(PC)_3$	−2.11
12	$Li^+(EC)_2(PC)_1$	−2.58	26	$Cs^+(EC)_2(PC)_1$	−2.78
13	$Li^+(EC)_2(PC)_2$	−2.02	27	$Cs^+(EC)_2(PC)_2$	−2.14
14	$Li^+(EC)_3(PC)_1$	−2.05	28	$Cs^+(EC)_3(PC)_1$	−2.17

lower LUMO energy of a molecule indicates it has a higher reductive potential. The results suggest that these Cs^+-solvates would serve as the preferred interphase precursor and experience the electrochemical reduction at the graphite surface before any Li^+-solvates do, leading to an SEI that bears heavy chemical signature from these Cs^+-solvates.

In PC-rich electrolytes such as E1Cs, the enrichment of EC around Cs^+ naturally leads to an EC-dominant SEI, despite the PC-presence in the bulk or in the solvation sheath of Li^+. Furthermore, an advantageous spatial factor may also play a role. The solvation structure of Li^+-$(EC)_a(PC)_b$ ($0 \leq a, b \leq 4$, and $a + b = 4$) solvates has a tetrahedron configuration (Figure 4B-a,b), while Cs^+-$(EC)_m$ (m = 1−3) solvates are most likely planar (Figure 4B-c), the consequence of which is that the latter would experience a much lower kinetic barrier in the initial cointercalation stages into edge sites of graphite with a spacing of 3.35 Å.[25] All of these factors combined lead to an SEI directed by the Cs^+-solvation sheath that is believed to be Cs^+-$(EC)_m$ (m = 1−2), which is schematically depicted in Figure 5. It has been reported (and predicted by the solvation-driven SEI model) that the SEI quality suffers from the Li^+ preference of PC over EC. By introducing Cs^+ at an additive

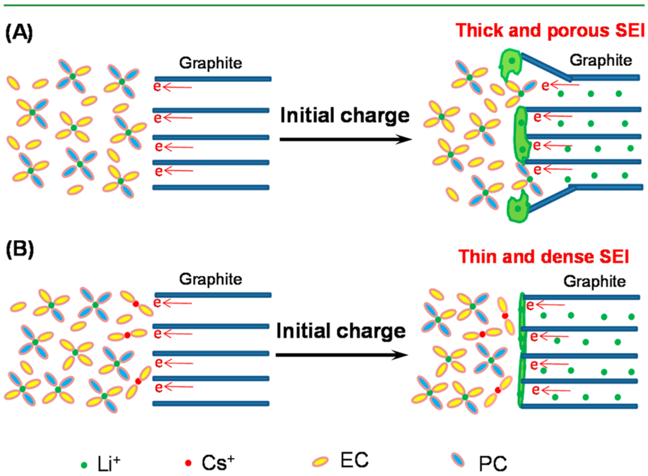

Figure 5. Schematic mechanism of SEI film formation promoted by Cs^+. (A) In a conventional electrolyte, Li^+ favors PC to form solvates. (B) In a Cs^+-containing electrolyte, due to the preferential formation of Li^+-$(PC)_n$ solvates, Cs^+ coordinates with EC molecules, and its solvates have priority to be electrochemically reduced.

level, the above undesired scenario is reversed. It should be noted that Cs^+ at 0.05 M has an effective redox potential of −3.103 V vs standard hydrogen electrode, lower than that of Li^+ at 1.0 M (−3.040 V vs standard hydrogen electrode);[14] thus Cs^+ will not be reduced at the working voltage (0.005 V cutoff) and the low charge current densities (C/20 rate). The reduced EC molecules probably would be converted into lithium or cesium salts of alkyl carbonates.[5]

Characterization of Interfacial Layers on Graphite Directed by Cs^+. The morphologies, structures, and chemical compositions of SEIs formed on graphite anodes were investigated by examining the graphite electrodes recovered from the Li||graphite cells initially charged to 0.3 V vs Li/Li^+ using various ex situ analytic means. At the chosen voltage, SEI should have been generated without Li^+ intercalation. Microbeam XRD performed on the graphite revealed that the (002) peaks remained the same as in the pristine sample (Figure 6A and Table S3). Even a high Cs^+ concentration (0.5 M) did not change the graphite bulk significantly (Figure S7). Hence, neither Li^+ nor Cs^+ intercalated into the graphitic structure at ≥0.3 V, and the main difference between various graphite electrodes is their surface chemistry. The graphite from E1 shows an increasing intensity below 20°, which is typical for exfoliated graphite or graphene.[26] The SEM images are shown in Figure 6B−E. The pristine graphite has a relatively clean surface (Figure 6B). The graphite from the cells using the E1 electrolyte shows significant deposits attached at its surface (Figure 6C), which should be the reductive decomposition products of electrolyte components. However, the graphite electrode from the E1Cs electrolyte has a clean surface with only limited spots (Figure 6D), which is similar to the pristine graphite. This suggests an ultrathin and uniform SEI layer on the graphite surface charged in the E1Cs electrolyte. Figure 6E shows many small spots embedded in the SEI layer on the graphite electrode in the E1FEC electrolyte.

The SEIs on these charged graphite electrodes (cutoff at 0.3 V) were further analyzed by high-resolution TEM. As shown in Figure 7A, the graphite particle in E1 is covered by a thick SEI with the thickness of >6 nm just after the initial charging process without lithiation. Both this thick SEI layer and the deposits shown in Figure 6C resulted from the extensive reductive decomposition of electrolyte components, PC solvent in particular. Graphite exfoliation also can be readily identified in this electrode, as labeled by yellow arrows in Figure S8. When FEC is present, a thin (2−4 nm), but uneven, SEI film covered the graphite surface (Figure 7B). An ultrathin (∼1 nm) and uniform SEI layer was found only in E1Cs (Figure 7C). This result is consistent with the SEM image in Figure 6D. It is also interesting to note that the edge plane of the graphite is intact without a thick film coverage and graphite exfoliation.

The chemical compositions of these interphases were analyzed by XPS (Figure 7D). The pristine graphite shows only C and F 1s nuclei, which arise from elemental carbon in the graphite and fluorine in the polyvinylidene difluoride binder, respectively. The abundance of C 1s decreases significantly in graphite surfaces recovered from cycled cells, suggesting that the original graphite surface had been covered by an interphase rich in other elements. On the basis of studies of SEIs, the main components of a common SEI layer include lithium carbonate, lithium alkyl carbonate, and other lithium salts. For the SEI formed in E1Cs, the higher C content and the lower Li content than those formed in E1 and E1FEC suggest that the SEI layer formed in E1Cs consists of more organic

DOI: 10.1021/acsami.5b05552
ACS Appl. Mater. Interfaces 2015, 7, 20687−20695

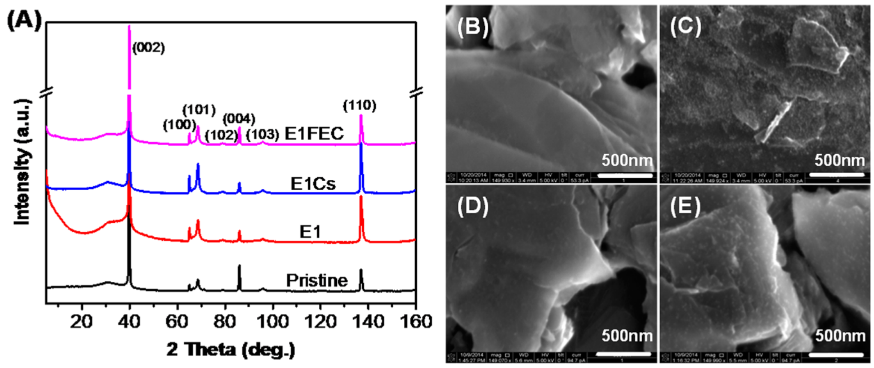

Figure 6. (A) Micro-XRD patterns of the graphite electrodes charged to 0.3 V in various electrolytes. (B−E) SEM images of graphite electrodes: (B) pristine graphite and (C−E) graphite electrodes charged to 0.3 V in electrolytes of E1 (C), E1Cs (D), and E1FEC (E).

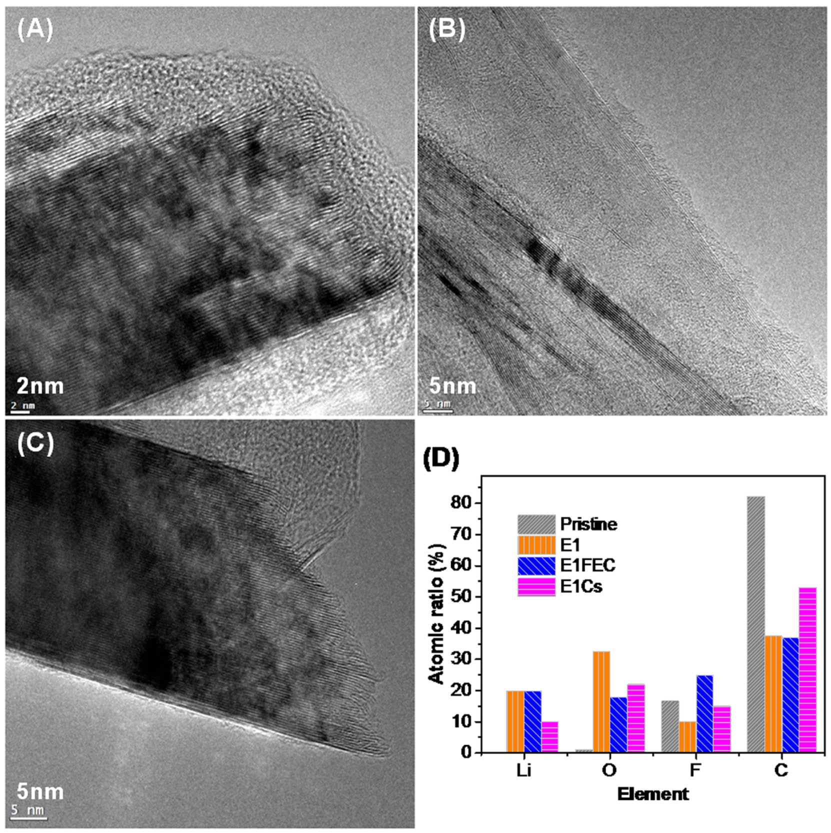

Figure 7. TEM images (A−C) and XPS results (D) of the graphite electrodes charged to 0.3 V from (A) E1, (B) E1FEC, and (C) E1Cs.

species than inorganic species. The ToF-SIMS results shown in Figure S9 also confirm that the SEI formed in E1Cs contains more oxygen while the SEI formed in E1FEC is rich in F.

Cell Performance of Graphite|NCA Full Cells with Cs^+. The performance advantages of Cs^+-directed interphases were demonstrated using full Li-ion cells based on graphite|NCA. Prior to testing in full cells, the electrolytes were tested in Li|NCA half cells (Figure S10), and the results show high Coulombic efficiency and good cycling stability for the Cs^+-electrolyte, indicating the stability of $CsPF_6$ up to at least 4.3 V and compatibility with the NCA cathode. As shown in Figure S11 and Figure 8, the full cells with E1Cs exhibit much better battery performances than those with E1 (without any additive) and even E1FEC in terms of Coulombic efficiency (Figure S11), cycling stability at both room temperature (Figure 8A) and elevated temperature (60 °C) (Figure 8B), and rate capability (Figure 8C).

E1 only delivers a low capacity <50 mAh g^{-1} after the formation cycles (Figure 8A), due to the extensive PC reduction (Figure 1A) and graphite exfoliation (Figure S8). The addition of $CsPF_6$ or FEC successfully suppressed PC reduction (Figure 1A). The fact that the $CsPF_6$ additive leads to better performance than FEC additive can be explained by the morphologies of the SEI films on graphite anodes after cycling (Figure 8D). After 100 cycles at 60 °C, the graphite anode from E1Cs appears to be clean, and the SEI layer is rather uniform with a thickness of ~1.5 nm (Figure 8D-a,c). This is almost the same as the SEI thickness generated at 0.3 V following the first charge (Figure 7C), indicating almost a constant interphasial morphology even at high temperature for long-term cycling. However, the SEI layer on the graphite from E1FEC contains

DOI: 10.1021/acsami.5b05552
ACS Appl. Mater. Interfaces 2015, 7, 20687−20695

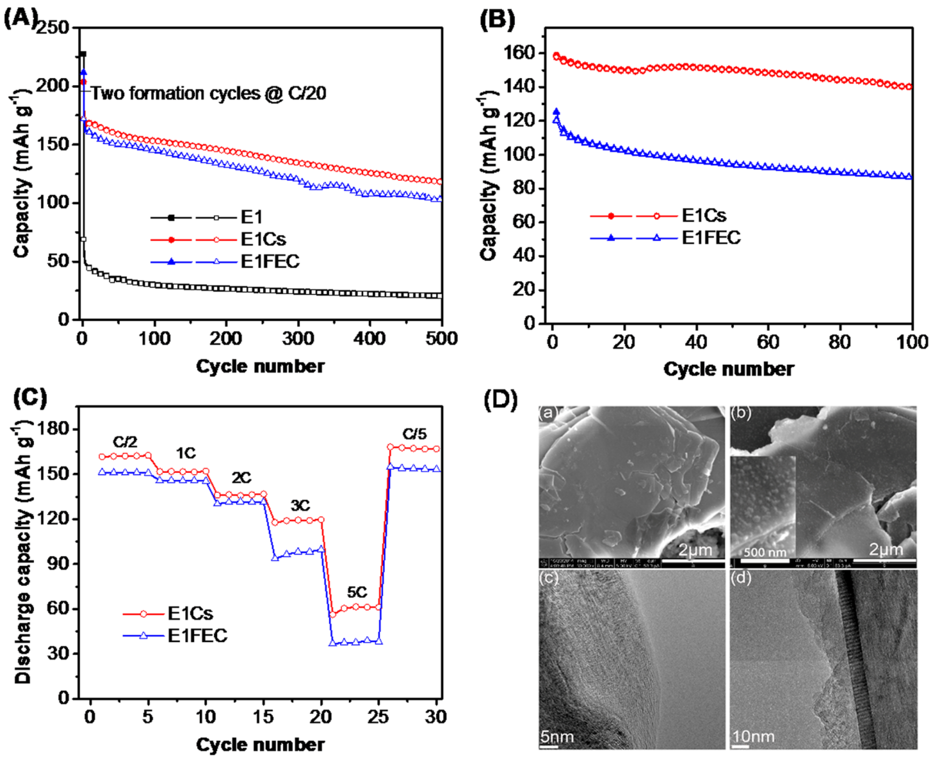

Figure 8. (A–C) Cell performances of graphite|NCA full cells and (D) SEM/TEM images of graphite anodes after 100 cycles at 60 °C. (A) Cycling performance at room temperature. Cells were charged at C/3 rate to 4.3 V and discharged at 1C rate to 2.5 V after 2 formation cycles. (B) Cycling performance at elevated temperature (60 °C). Cells were charged and discharged at C/2 after 2 formation cycles at room temperature. (C) Rate capability at room temperature. Cells were charged at C/5 and then discharged at various C-rates. (D) SEM images of graphite anodes from the graphite|NCA cells with E1Cs (a) or E1FEC (b), and TEM images of the SEI layers on graphite anodes from the graphite|NCA cells with E1Cs (c) or E1FEC (d).

many particles, and the thickness is uneven between 11 and 28 nm (Figure 8D-b,d). E1Cs also exhibits a room-temperature cycling stability comparable to the state-of-the-art electrolyte E2 and better than another electrolyte E1VC with 2% VC (Figure S12A). The latter control electrolytes also show poor cycling stability at elevated temperature (Figure S12B).

The above Cs^+-effect on interphase could be extended to other electrolyte formulations. Figure S13 shows that the addition of 0.04 M $CsPF_6$ in an electrolyte of 1 M $LiPF_6$/EC-PC-EMC (2:1:7 by wt) can improve the first cycle Coulombic efficiency of graphite|NCA full cells from 79% to 84% as well as the high-temperature cycling stability. More importantly, significantly improvements of low temperature performances at −30 and −40 °C were also achieved by the Cs^+-directed interphase when compared to the state-of-the-art electrolyte E2 (Figure S14). The high capacity retention at such low temperatures apparently benefited from the ultrathin SEI layer and its low impedance (Figure S15).

4. CONCLUSIONS

Cs^+ in nonaqueous electrolytes acts as a core that directs the formation chemistry of SEI. Detailed investigations showed that Cs^+ as a weak Lewis acid has a lower solvation number and is less competitive with the stronger solvating PC molecule. In a PC-rich electrolyte, the coexistence of Li^+ and Cs^+ would suggest a primarily EC-dominant solvation sheath of the latter. Solvates of Cs^+-$(sol)_m$ ($1 \leq m \leq 2$) have faster transport rates because of their smaller ionic sizes than the Li^+-$(sol)_n$ ($3 \leq n \leq 5$) solvates, and they also have lower LUMO energies. Therefore, at the initial forming stage of interphase reactions, EC molecules enriched by a Cs^+ core would become the most probable SEI-precursor, leading to protection of the graphitic anode in a PC-rich environment. The ultrathin and compact SEI directed by Cs^+ can significantly reduce cell impedance, thus enhancing the cycling stability at elevated temperatures, the rate capability, and the low-temperature discharge performance of LIBs down to −40 °C. This new approach of exercising precise control over the formation chemistry of the interphase can be more practically applied in commercial LIBs to enable many applications that are otherwise impossible.

■ ASSOCIATED CONTENT

Supporting Information

The Supporting Information is available free of charge on the ACS Publications website at DOI: 10.1021/acsami.5b05552.

Information and figures about electrodes and electrolytes, micro-XRD spectra and analysis, additional ESI–MS results, solvation energies, optimized solvate structures, SEM and TEM images, ToF-SIMS results, and battery performance (PDF)

■ AUTHOR INFORMATION

Corresponding Author

*E-mail: wu.xu@pnnl.gov.

Author Contributions

W.X. and H.X. conceived and designed the experiments with the help from J.-G.Z. and K.X. H.X. prepared the samples and performed the electrochemical measurements with the help from R.C. D.M. did the DFT calculations, P.Y. and C.-M.W.

performed TEM, P.B. conducted SEM and EDX tests, M.H.E. carried out the XPS analysis, M.E.B. measured the micro-XRD, Z.Z. did the ToF-SIMS, S.D.B. did ^{17}O NMR tests, A.V.C and K.X. performed the ESI−MS, and B.J.P. prepared the graphite and NCA electrodes. H.X. and W.X. proposed the explanations and the mechanism for the Cs^+-assisted SEI formation. H.X., W.X., J.-G.Z., and K.X. prepared the manuscript with the input from all other coauthors. All authors have given approval to the final version of the manuscript.

Notes

The authors declare no competing financial interest.

■ ACKNOWLEDGMENTS

This work was supported by the Assistant Secretary for Energy Efficiency and Renewable Energy, Office of Vehicle Technologies, the Advanced Battery Materials Research (BMR) programs of the U.S. Department of Energy (DOE) under contract no. DE-AC02-05CH11231, subcontract no. 18769. The microscopic images and spectroscopic measurements were conducted in the William R. Wiley Environmental Molecular Sciences Laboratory, a national scientific user facility sponsored by the DOE's Office of Biological and Environmental Research and located at Pacific Northwest National Laboratory (PNNL). Computing time was granted by the National Energy Research Scientific Computing Center. We thank Mr. Yufan Zhou for help in the ToF-SIMS analysis. H.X. acknowledged financial support from the National Science Foundation of China (Grant nos. 21006033 and 51372060) and Fundamental Research Funds for the Central Universities (2013HGCH0002). P.B. gratefully acknowledged support from the Linus Pauling distinguished Postdoctoral Fellowship from PNNL. K.X. acknowledged the support from U.S. DOE under the Interagency Agreement no. DE-EE0006543. PNNL is operated by Battelle for the DOE under contract DE-AC05-76RLO1830.

■ REFERENCES

(1) Xu, K. Nonaqueous Liquid Electrolytes for Lithium-Based Rechargeable Batteries. *Chem. Rev.* **2004**, *104*, 4303−4417.

(2) Ohtaki, H. Structural Studies on Solvation and Complexation of Metal Ions in Nonaqueous Solutions. *Pure Appl. Chem.* **1987**, *59*, 1143−1150.

(3) Yamada, Y.; Iriyama, Y.; Abe, T.; Ogumi, Z. Kinetics of Lithium Ion Transfer at the Interface between Graphite and Liquid Electrolytes: Effects of Solvent and Surface Film. *Langmuir* **2009**, *25*, 12766−12770.

(4) Xu, K. Charge-Transfer" Process at Graphite/Electrolyte Interface and the Solvation Sheath Structure of Li^+ in Nonaqueous Electrolytes. *J. Electrochem. Soc.* **2007**, *154*, A162−A167.

(5) Xu, K.; Lam, Y.; Zhang, S. S.; Jow, T. R.; Curtis, T. B. Solvation Sheath of Li^+ in Nonaqueous Electrolytes and its Implication of Graphite/Electrolyte Interface Chemistry. *J. Phys. Chem. C* **2007**, *111*, 7411−7421.

(6) Jeong, S.-K.; Inaba, M.; Iriyama, Y.; Abe, T.; Ogumi, Z. Electrochemical Intercalation of Lithium Ion within Graphite from Propylene Carbonate Solutions. *Electrochem. Solid-State Lett.* **2003**, *6*, A13−A15.

(7) Jeong, S.-K.; Inaba, M.; Iriyama, Y.; Abe, T.; Ogumi, Z. Interfacial Reactions between Graphite Electrodes and Propylene Carbonate-Based Solutions: Electrolyte-Concentration Dependence of Electrochemical Lithium Intercalation Reaction. *J. Power Sources* **2008**, *175*, 540−546.

(8) Yamada, Y.; Takazawa, Y.; Miyazaki, K.; Abe, T. Electrochemical Lithium Intercalation into Graphite in Dimethyl Sulfoxide-Based Electrolytes: Effect of Solvation Structure of Lithium Ion. *J. Phys. Chem. C* **2010**, *114*, 11680−11685.

(9) Takeuchi, S.; Miyazaki, K.; Sagane, F.; Fukutsuka, T.; Jeong, S.-K.; Abe, T. Electrochemical Properties of Graphite Electrode in Propylene Carbonate-Based Electrolytes Containing Lithium and Calcium Ions. *Electrochim. Acta* **2011**, *56*, 10450−10453.

(10) Takeuchi, S.; Fukutsuka, T.; Miyazaki, K.; Abe, T. Electrochemical Preparation of a Lithium−Graphite-Intercalation Compound in a Dimethyl Sulfoxide-Based Electrolyte Containing Calcium Ions. *Carbon* **2013**, *57*, 232−238.

(11) Frisch, M. J.; Trucks, G. W.; Schlegel, H. B.; Scuseria, G. E.; Robb, M. A.; Cheeseman, J. R.; Scalmani, G.; Barone, V.; Mennucci, B.; Petersson, G. A.; Nakatsuji, H.; Caricato, M.; Li, X.; Hratchian, H. P.; Izmaylov, A. F.; Bloino, J.; Zheng, G.; Sonnenberg, J. L.; Hada, M.; Ehara, M.; Toyota, K.; Fukuda, R.; Hasegawa, J.; Ishida, M.; Nakajima, T.; Honda, Y.; Kitao, O.; Nakai, H.; Vreven, T.; Montgomery, J. A., Jr.; Peralta, J. E.; Ogliaro, F.; Bearpark, M. J.; Heyd, J.; Brothers, E. N.; Kudin, K. N.; Staroverov, V. N.; Kobayashi, R.; Normand, J.; Raghavachari, K.; Rendell, A. P.; Burant, J. C.; Iyengar, S. S.; Tomasi, J.; Cossi, M.; Rega, N.; Millam, N. J.; Klene, M.; Knox, J. E.; Cross, J. B.; Bakken, V.; Adamo, C.; Jaramillo, J.; Gomperts, R.; Stratmann, R. E.; Yazyev, O.; Austin, A. J.; Cammi, R.; Pomelli, C.; Ochterski, J. W.; Martin, R. L.; Morokuma, K.; Zakrzewski, V. G.; Voth, G. A.; Salvador, P.; Dannenberg, J. J.; Dapprich, S.; Daniels, A. D.; Farkas, Ö.; Foresman, J. B.; Ortiz, J. V.; Cioslowski, J.; Fox, D. J. *Gaussian 09*; Gaussian, Inc.: Wallingford, CT, 2009.

(12) Boys, S. F.; Bernardi, F. The Calculation of Small Molecular Interactions by the Differences of Separate Total Energies. Some Procedures with Reduced Errors. *Mol. Phys.* **1970**, *19*, 553−566.

(13) Lee, C.; Yang, W.; Parr, R. G. Development of the Colle-Salvetti Correlation-Energy Formula into a Functional of the Electron Density. *Phys. Rev. B: Condens. Matter Mater. Phys.* **1988**, *37*, 785−789.

(14) Ding, F.; Xu, W.; Graff, G. L.; Zhang, J.; Sushko, M. L.; Chen, X. L.; Shao, Y. Y.; Engelhard, M. H.; Nie, Z. M.; Xiao, J.; Liu, X. J.; Sushko, P. V.; Liu, J.; Zhang, J.-G. Dendrite-Free Lithium Deposition via Self-Healing Electrostatic Shield Mechanism. *J. Am. Chem. Soc.* **2013**, *135*, 4450−4456.

(15) von Cresce, A.; Xu, K. Preferential Solvation of Li^+ Directs Formation of Interphase on Graphitic Anode. *Electrochem. Solid-State Lett.* **2011**, *14*, A154−A156.

(16) Xu, K.; von Wald Cresce, A. Li^+-Solvation/Desolvation Dictates Interphasial Processes on Graphitic Anode in Li Ion Cells. *J. Mater. Res.* **2012**, *27*, 2327−2341.

(17) von Wald Cresce, A.; Borodin, O.; Xu, K. Correlating Li^+ Solvation Sheath Structure with Interphasial Chemistry on Graphite. *J. Phys. Chem. C* **2012**, *116*, 26111−26117.

(18) Cazzanelli, E.; Croce, F.; Appetecchi, G. B.; Benevelli, F.; Mustarelli, P. Li^+ Solvation in Ethylene Carbonate−Propylene Carbonate Concentrated Solutions: A Comprehensive Model. *J. Chem. Phys.* **1997**, *107*, 5740−5747.

(19) Yanase, S.; Oi, T. Solvation of Lithium Ion in Organic Electrolyte Solutions and Its Isotopie Reduced Partition Function Ratios Studied by ab initio Molecular Orbital Method. *J. Nucl. Sci. Technol.* **2002**, *39*, 1060−1064.

(20) Blint, R. J. Binding of Ether and Carbonyl Oxygens to Lithium Ion. *J. Electrochem. Soc.* **1995**, *142*, 696−702.

(21) Wang, Y.; Nakamura, S.; Ue, M.; Balbuena, P. B. Theoretical Studies to Understand Surface Chemistry on Carbon Anodes for Lithium-Ion Batteries: Reduction Mechanisms of Ethylene Carbonate. *J. Am. Chem. Soc.* **2001**, *123*, 11708−11718.

(22) Bhatt, M. D.; O'Dwyer, C. The Role of Carbonate and Sulfite Additives in Propylene Carbonate-Based Electrolytes on the Formation of SEI Layers at Graphitic Li-Ion Battery Anodes. *J. Electrochem. Soc.* **2014**, *161*, A1415−A1421.

(23) Chen, X.; Xu, W.; Engelhard, M. H.; Zheng, J.; Zhang, Y.; Ding, F.; Qian, J.; Zhang, J.-G. Mixed Salts of LiTFSI and LiBOB for Stable $LiFePO_4$-Based Batteries at Elevated Temperatures. *J. Mater. Chem. A* **2014**, *2*, 2346−2352.

(24) Bogle, X.; Vazquez, R.; Greenbaum, S.; Cresce, A. v. W.; Xu, K. Understanding Li^+−Solvent Interaction in Nonaqueous Carbonate Electrolytes with ^{17}O NMR. *J. Phys. Chem. Lett.* **2013**, *4*, 1664−1668.

DOI: 10.1021/acsami.5b05552
ACS Appl. Mater. Interfaces 2015, 7, 20687−20695

(25) Wagner, M. R.; Albering, J. H.; Moeller, K. C.; Besenhard, J. O.; Winter, M. XRD Evidence for the Electrochemical Formation in PC-Based Electrolytes. *Electrochem. Commun.* **2005**, *7*, 947−952.
(26) Grayfer, E. D.; Nazarov, A. S.; Makotchenko, V. G.; Kim, S.-J.; Fedorov, V. E. Chemically Modified Graphene Sheets by Functionalization of Highly Exfoliated Graphite. *J. Mater. Chem.* **2011**, *21*, 3410−3414.

DOI: 10.1021/acsami.5b05552
ACS Appl. Mater. Interfaces 2015, 7, 20687−20695